Effects of asymmetry and hot-spot shape on ignition capsules

B. Cheng,[1,*] T. J. T. Kwan,[1] S. A. Yi,[1] O. L. Landen,[2] Y. M. Wang,[1] C. J. Cerjan,[2] S. H. Batha,[1] and F. J. Wysocki[1]

[1]*Los Alamos National Laboratory, Los Alamos, New Mexico 87545, USA*

[2]*Lawrence Livermore National Laboratory, Livermore, California 94550, USA*

Asymmetric implosion of inertial confinement fusion capsules is known, both experimentally and computationally, to reduce thermonuclear performance. This work shows that low-mode asymmetries degrade performance as a result of a decrease in the hydrodynamic disassembly time of the hot-spot core, which scales with the minimum dimension of the hot spot. The asymmetric shape of a hot spot results in decreased temperatures and areal densities and allows more alpha particles to escape, relative to an ideal spherical implosion, thus reducing alpha-energy deposition in the hot spot. Here, we extend previous ignition theory to include the hot-spot shape and quantify the effects of implosion asymmetry on both the ignition criterion and the capsule performance. The ignition criterion becomes more stringent with increasing deformation of the hot spot. The new theoretical results are validated by comparison with existing experimental data obtained at the National Ignition Facility. The shape effects on thermonuclear performance are relatively more noticeable for capsules having self-heating and high yields. The degradation of thermonuclear burn can be as high as 45% for shots with a yield lower than 2×10^{15} and less than 30% for shots with a higher yield.

I. INTRODUCTION

High-convergence inertial confinement fusion (ICF) implosions at the National Ignition Facility (NIF) frequently deviate from their desired one-dimensional (1D) spherical state, resulting in degradation of the fusion energy output. The physics of implosion asymmetry has been studied for many years [1,2]. It has been demonstrated that the implosion asymmetry must be less than a few percent ($\sim$3%$-$4%) [1–3] in order to achieve the densities and temperatures required for thermonuclear ignition and burn. Therefore, it is critical to improve the fuel target implosion symmetry and to maintain a spherically uniform target compression. In general, the implosion asymmetry is caused by the driver-beam nonuniform illumination, which leads to ablation pressure inhomogeneity, nonuniform radiation flux, and features such as structural perturbations on the capsule surface, imperfect target sphericity, a nonuniform target density, target alignment errors, small low-mode aymmetries in the initial capsule shape, and the presence of the capsule support tent and fill tube. Experimental evidence shows that these asymmetries result in changes in the in-flight shape of the capsule and in the final hot-spot shape, leading to reduced thermonuclear performance [1,2,4–9].

Effects of nonuniform implosion on the drive pressure symmetry and fusion performance were investigated numerically in the 1980s [1,2]. It was discovered that laser nonuniformities with scale lengths greater than the distance from the ablation surface to the critical surface would have a severe impact on the symmetry of the drive pressure and target compression and, in turn, the shape of the hot spot. The maximum degradation of nonuniform implosion on the fusion parameters, namely, on the areal density, the peak mass density and ion temperature

of the hot deuterium-tritium (DT) fuel after implosion, and the thermonuclear energy output, is less than 50% for 100% spatial variations of physical quantities, such as the radius, the implosion velocity, and the number density of the hot DT fuel [2]. It was shown that the influence of low-mode asymmetry on the fusion parameters is slightly more significant in comparison with that of high-mode asymmetry.

Impacts of the hot-spot shape at the time of stagnation on the nuclear performance of NIF ignition capsules have also been studied numerically in recent years [10–12], but the physical relationship between hot-spot shape and thermonuclear burn has not been systematically studied. A recent computational study evaluated hot-spot asymmetries resulting in implosion desynchronization and reduced fuel compression, but the thermonuclear phase was not considered [9,13–16]. Additionally, 2D and 3D numerical simulations have suggested that asymmetries of the hot spots would significantly reduce the experimental yield [5].

In this article, we determine the effects of hot-spot shape at late times on the alpha-particle deposition and neutron yield of capsules. We extend our ignition theory [17–21] to include the hot-spot shape and quantify the effects of implosion asymmetry on both the ignition criterion and the capsule performance. Theoretical results are validated by comparison with existing NIF experimental data. The results explain the correlation between hot-spot shape and neutron yield of fusion capsules.

II. HOT SPOT SHAPES

ICF experimental data indicate that the hot spot in an ignition capsule is often symmetric with respect to the axis of the hohlraum; i.e., the polar view of the hot spot is almost always within 20% of circular and sometimes ringlike. The equatorial view of the hot spot ranges from round to oblate or prolate. The ring shape in the polar view is an implosion defect,
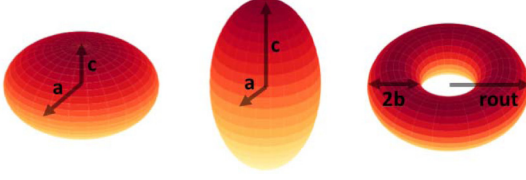
023203-1

FIG. 1. Hot-spot shapes considered: oblate (left), prolate (middle), and torus (right). The sphere and dipole are not plotted.

probably caused by a polar jet or collisions of incoming and reflected shocks during the implosion. This defect could be minimized or removed by carefully controlling the shock and reflected shock in the implosion design. It is noteworthy that NIF "toroidal" implosions do not create true toroids. The polar emissivity (x ray or neutron) does not go to 0. So a toroidal hot spot on a nuclear image is, in fact, more a depression than a true void. The same is true for a dipole configuration (a dipole hot spot is composed of two isolated spheres at the poles). For simplicity, we consider five geometric hot-spot shapes: sphere, oblate, prolate, torus, and dipole. The oblate, prolate, and torus shapes are displayed in Fig.1.

The equation of a spheroid centered at the origin with z as the symmetry axis is

$$\frac{x^2 + y^2}{a^2} + \frac{z^2}{c^2} = 1, \tag{1}$$

where x, y, and z are Cartesian coordinates, a is the equatorial radius of the spheroid, and c is the distance from center to pole (polar radius) along the symmetry axis. If $c = a$, the spheroid is a sphere, if $c < a$, the spheroid becomes oblate, and if $c > a$, the spheroid will be prolate. The volume of a spheroid is given by the expression

$$V_{\text{sph}} = 4\pi a^2 c/3. \tag{2}$$

The equation of a torus azimuthally symmetric with respect to the z axis is

$$(d - \sqrt{x^2 + y^2})^2 + z^2 = b^2, \tag{3}$$

where d is the radius from the center of the hole to the center of the torus tube and b is the radius of the torus tube. The volume of a torus is

$$V_{\text{tor}} = 2\pi^2 b^2 d. \tag{4}$$

In terms of the inner and outer radii, $r_{\text{in}} \equiv d - b$ and $r_{\text{out}} \equiv d + b$, the volume of the torus can also be written as

$$V_{\text{tor}} = \frac{1}{4}\pi^2 (r_{\text{out}} + r_{\text{in}})(r_{\text{out}} - r_{\text{in}})^2. \tag{5}$$

In experiments, the equatorial images (neutron and x ray) of a hot spot is fitted with Legendre polynomials to characterize the size and shape of each neutron source distribution and x-ray-emitting core, The results of this fit provide a measure of the lowest mode of hot-spot asymmetry, P_2/P_0, which is the ratio of the second-order to the zeroth-order Legendre polynomials that are required to fit the contour at 17% of the peak neutron emission. Contributions from higher-order modes are similarly determined. In terms of P_2 and P_0 and by definition, the equatorial radius is $a = P_0 - P_2/2$ and the polar radius is $c = P_0 + P_2$. For a prolate hot spot, $P_2 > 0$, and for

an oblate one, $P_2 < 0$. Thus, the aspect ratio a/c of a spheroid, i.e., the ratio of the equatorial radius a to the distance from the center to the pole c, is given as $a/c = [1 - P_2/(2P_0)]/(1 + P_2/P_0)$. For small P_2/P_0, $a/c \simeq 1 - 3P_2/(2P_0)$.

III. SHAPE DEPENDENT HYDRODYNAMIC DISASSEMBLY TIME

Hot-spot ICF ignition relies on thermonuclear burn initiation in the hot spot and robust burn propagation to the rest of the cold fuel. For self-sustained burn to occur in the hot spot, the resultant alpha particles must be captured in the hot spot and heat the DT gas. The thermonuclear burn efficiency of the hot spot directly depends on the alpha heating process in the hot spot through alpha-particle deposition and hot-spot hydrodynamic disassembly. Ignition requires that the hot-spot nuclear reproduction time be less than the hot-spot hydrodynamic disassembly time, resulting in the temperature runaway phenomenon [17,18]. Both the nuclear reproduction time via alpha-particle energy deposition and the hot-spot hydrodynamic disassembly time are sensitive to the geometric shape of the hot spot. It is clear that the hydrodynamic disassembly time is at its minimum in the direction of the shortest dimension of the hot spot. A shorter hydrodynamic disassembly time in one direction will cause a shorter time for overall nuclear reproduction and a shorter time for alpha-heating in the entire hot spot. Additionally, radiation energy, thermal conduction, and alpha particles are preferentially lost from the system in the same direction, without depositing their energy [22,23].

The thermonuclear confinement of the hot spot in an ICF capsule is directly associated with the hydrodynamic disassembly time, which is determined by the shortest dimension of the hot spot divided by the sound speed in the hot spot. The longer the thermonuclear confinement, the larger the burn fraction of the DT fuel, and the closer the thermonuclear burn to ignition. Therefore, the shape of the hot spot should play a role in thermonuclear burn and capsule performance via hydrodynamic disassembly and confinement.

We begin by establishing a relationship between the shortest geometric dimension of the hot spots shown in Fig. 1 and a 1D perfect sphere. When a two-dimensional analysis is appropriate, we assume that the 2D projected area in the equatorial view, $r_0^2 = ac$, is conserved among the different shapes. When a three-dimensional analysis is appropriate, we assume that the volume of the hot spots, $r_0^3 = a^2 c$, is conserved (where r_0 is the radius of the 1D sphere). Under these assumptions, we are able to obtain the relationship between the radius of the 1D sphere and the dimensional parameters of the spheroids or torus. These assumptions are supported by the results of the analysis shown later.

Conserving the projected area of a 2D prolate hot spot in the equatorial view leads to

$$a = r_0\sqrt{a/c} = r_0\sqrt{\frac{1 - P_2/(2P_0)}{1 + P_2/P_0}}. \tag{6}$$

For an oblate hot spot, the expression for the polar radius is $c = r_0\sqrt{(1 + P_2/P_0)/[1 - P_2/(2P_0)]}$. Note that an equatorial projection does not distinguish between a torus and an oblate spheroid; a torus hot spot would have similar equatorial

projections in the 2D equatorial view. Thus, for all hot-spot shapes, the ratio of the shortest radius ($r_{\min}$) to the radius of a 1D sphere has the same expression,

$$\frac{r_{\min}}{r_0} = g_{2D}, \tag{7}$$

where g_{2D} is a function of the shape of the two-dimensional hot spot:

$$g_{2D} \equiv \begin{cases} \left(\frac{1-P_2/(2P_0)}{1+P_2/P_0}\right)^{1/2}, & \text{prolate}; \\ \left(\frac{1-|P_2/P_0|}{1+|P_2/P_0|/2}\right)^{1/2}, & \text{oblate}. \end{cases} \tag{8}$$

For small $|P_2/P_0|$, $g_{2D} \simeq \sqrt{1-3|P_2/P_0|/2}$ for all shapes. For any given P_2/P_0, the g_{2D} of a prolate hot spot is always greater than the g_{2D} of an oblate hot spot.

For 3D hot spots, we assume that the hot-spot volume, $r_0^3 = a^2 c \equiv a^3(c/a)$, is conserved (i.e., the hot-spot volume is the same for all shapes). Under this assumption, toroidal, prolate, oblate, and dipolar hot spots are distinguishable. For oblate hot spots ($c < a$), the relationship between the shortest equatorial radius $r_{\min}$ and a 1D sphere of radius r_0 is

$$c = r_0 \left(\frac{1-|P_2/P_0|}{1+|P_2/P_0|/2}\right)^{2/3}. \tag{9}$$

For prolate hot spots ($c > a$), the relationship takes the form

$$a = r_0 \left[\frac{1-P_2/(2P_0)}{1+P_2/P_0}\right]^{1/3}. \tag{10}$$

The equatorial view of a toroidal shape is similar to an oblate hot spot and can also be described by Legendre polynomials. The aspect ratio can be expressed as $b/r_{\text{out}} \simeq (1+P_2/P_0)/[1-P_2/(2P_0)]$. By conserving the volume of the hot spot, we obtain an expression for the shortest dimension of a toroidal hot spot, i.e., the radius of the torus in terms of the 1D sphere radius

$$b = r_0 \left[\frac{2}{3\pi (r_{\text{out}}/b - 1)}\right]^{1/3}. \tag{11}$$

By definition, the radius of a torus has to be less than $r_{\text{out}}/2$ for $d > b$ to have a hole; this constraint gives the bound $P_2/P_0 < -0.4$ for a toroidal hot spot. At $P_2/P_0 = -0.4$, $b \simeq 0.6 r_0$, which is the maximum height of the torus in terms of r_0. Legendre expression shows that for values of P_2/P_0 from -0.5 to -1.0, the variation of the height of a torus stays within $\pm 4\%$ of $0.6 P_0$. Therefore, we use the approximation $b/r_{\text{out}} \approx 0.6/(1+|P_2/P_0|/2)$ for a toroidal hot spot in our analysis.

Since the density profile of a toroidal hot spot does not really go to 0 at the center, one can treat the toroid as an oblate object with a density depression at the center. The topology of an oblate hot spot changes to a toroid when $P_2/P_0 < -0.4$. Similarly, a hot spot with a prolate topology will become a dipole when $P_2/P_0 > 0.5$. At $P_2/P_0 = 0.5$, $a/c = [1 - P_2/(2P_0)]/(1+P_2/P_0) \simeq 1/2$, a prolate spheroid turns into a dipole with radius $a \simeq r_0(1/2)^{1/3} \simeq 0.8 r_0$. This radius remains for all values of $P_2/P_0 > 0.5$ if we assume that each end of the dipole approximates a sphere of radius $b \simeq a$. Thus, for a 3D hot spot, the ratio of the shortest dimension ($r_{\min}$) to the radius

of a 1D sphere can be expressed as $\frac{r_{\min}}{r_0} = g_{3D}$, where

$$g_{3D} \equiv \begin{cases} \left[\frac{1-P_2/(2P_0)}{1+P_2/P_0}\right]^{1/3}, & \text{prolate}, \\ \left(\frac{1-|P_2/P_0|}{1+|P_2/P_0|/2}\right)^{2/3}, & \text{oblate}, \\ \left[\frac{2}{3\pi}\left(\frac{0.6}{0.4+|P_2/P_0|/2}\right)\right]^{1/3}, & \text{torus}, \\ 0.8, & \text{dipole} \end{cases} \tag{12}$$

is a function of the geometric shape of the hot spot. Both Eq. (8) and Eq. (12) show that the shortest dimension of the hot spot decreases as the hot spot departs from a spherical shape. For any given P_2/P_0, the g_{3D} of a prolate hot spot is always greater than the g_{3D} of an oblate one. So prolate hot spots should perform better than oblate hot spots. This result is consistent with the experimental data obtained at NIF, discussed later. A more general function of geometric shape including contributions of P_4 and M_4 is given in the Appendix. In this article we focus on the effects of low-mode P_2.

As discussed earlier, the hydrodynamic disassembly time of deformed hot spots is a function of the hot-spot shape and is determined by the shortest dimension of the hot spot. The disassembly time can be expressed as

$$\tau_h^{2D} \equiv \frac{r_{\min}}{C_s} = \frac{r_0}{C_s} g_{2D} \equiv \tau_0 g_{2D} \tag{13}$$

for 2D hot spots and

$$\tau_h^{3D} \equiv \frac{r_{\min}}{C_s} = \frac{r_0}{C_s} g_{3D} \equiv \tau_0 g_{3D} \tag{14}$$

for 3D hot spots. The parameter $C_s = (2\gamma_g RT/A_{\text{DT}})^{1/2} \simeq 2.778 \times 10^7 \sqrt{\gamma_g T \text{ (keV)}}$ cm/s is the speed of sound in the hot spot. Here, γ_g is the adiabatic index of the hot deuterium-tritium fuel, A_{DT} is the atomic weight mass of the DT mixture, R is the gas constant, and T is the hot-spot temperature in keV. The hydrodynamic disassembly time of a perfect sphere is $\tau_0 \equiv r_0/C_s$. The shape functions g_{2D} and g_{3D} are given, respectively, by Eqs. (8) and (12).

IV. SHAPE DEPENDENT IGNITION CRITERION AND CAPSULE PERFORMANCE

From Eqs. (8) and (12), for oblate and toroidal hot spots with nonzero P_2/P_0, $g_{3D} \leqslant g_{2D} \leqslant 1$. Thus, $\tau_{3D} \leqslant \tau_{2D} < \tau_0$, which indicates that any ignition capsules departing from the 1D implosion symmetry would be less robust because of the shorter time available for self-sustained thermonuclear burn. So it would be more difficult for a 2D or a 3D capsule to achieve ignition. In order to quantify this point, we substitute the shape-dependent hydrodynamic disassembly time, Eq. (13) or (14), into the 1D thermonuclear ignition criterion [18,24] and obtain the shape-dependent ignition threshold for the areal density of the hot spot

$$(\rho r)_{\text{hs}}^i \geqslant (\rho r)_{\text{IT}}^{\text{1D}}/g_i, \tag{15}$$

where $i = 2D$ or $3D$, and $(\rho r)_{\text{IT}}^{\text{1D}}$ is the 1D ignition threshold on the hot-spot areal density, given by the expression [18]

$$(\rho r)_{\text{IT}}^{\text{1D}} \equiv \frac{[(1+d^*)^2/d^*][3kT + E_{\text{rad}}/n_{\text{DT}}]C_s A_{\text{DT}}/N_A}{\langle \sigma v \rangle_{\text{DT}} W_\alpha - (\dot{Q}_l^b + \dot{Q}_l^e)(1+d^*)^2/(d^* n_{\text{DT}}^2)}, \tag{16}$$

where $n_{\mathrm{DT}} \equiv n_{\mathrm{D}} + n_{\mathrm{T}} = \rho_{\mathrm{DT}} N_A / A_{\mathrm{DT}}$, $\dot{Q}_l^i \equiv dQ_l^i / dt$ $(i = b, e)$ represent the energy loss by electron bremsstrahlung and electron conduction, d^* is the D-to-T ratio, N_A is Avogadro's number, and k is the Boltzmann constant. The nuclear reactivity $\langle \sigma v \rangle_{\mathrm{DT}}$ [25,26] can be approximated by a power law of temperature, T^n. For the temperature range 3–5.5 keV, $\langle \sigma v \rangle_{\mathrm{DT}} \approx C_{\mathrm{DT}} T^4$ is a good approximation [18], where $C_{\mathrm{DT}} \simeq 2.3 \times 10^{-20}$ cm^3/s/keV^4. The shape function g_i is given by Eqs. (8) and (12) for 2D and 3D geometries, respectively. With $g_i < 1$, the ignition threshold for a 2D or 3D hot spot increases due to shape asymmetry. This result is consistent with the simulations performed by Kawata [2].

Similarly, the ignition parameter for 2D and 3D hot spots becomes $\chi_i \equiv P_{\mathrm{hs}} \tau_0 g_i / (P\tau)_{\mathrm{IT}}$, where $(P\tau)_{\mathrm{IT}} \equiv T^2$ (keV)$/(9.17 \times 10^{16} \langle \sigma v \rangle)$ is the ignition threshold in Gbarns. At $T = 4$ keV, $(P\tau)_{\mathrm{IT}} \simeq 29.7$ Gbar-ns [18]. Ignition occurs when

$$P_{\mathrm{hs}} \tau_h \geqslant (P\tau)_{\mathrm{IT}} / g_i. \tag{17}$$

Substituting the power-law solution of $\langle \sigma v \rangle$ [18] into Eqs. (16) and (17), we obtain the analytical form of the Lawson criterion for asymmetric imploding ignition capsules,

$$P(\mathrm{Gbar}) \tau_h \,(\mu\mathrm{s}) > \frac{2\kappa_c}{A_{\mathrm{DT}}} \frac{(1+d^*)^2}{d^*} \frac{0.03472}{\gamma_g^{1/2} g_i T \,(\mathrm{keV})^2}, \tag{18}$$

where κ_c is a fitting constant and has the value 5.514 [18]. The minimum required hot-spot mass for achieving sustained thermonuclear burn in 2D or 3D hot spots with $\langle \sigma v \rangle \sim T^4$ is given by

$$M_{\mathrm{hs}}^{\min} \geqslant \frac{4\pi}{3} \frac{\kappa_c}{g_i} \frac{(1+d^*)^2/d^*}{T \,(\mathrm{keV})^{2.5}} \frac{r_{0\mathrm{F}}^2}{C_f^2}, \tag{19}$$

where $C_f \equiv r_{0\mathrm{F}} / r_{\mathrm{hs}}$ is the geometric convergence ratio and $r_{0\mathrm{F}}$ and r_{hs} are, respectively, the initial inner radius of the fuel and the final radius of the hot spot.

The hot-spot pressure of an asymmetric hot spot is determined by the formula

$$P_{\mathrm{hs}}^i = 772 \times \left[\frac{8\pi (3\gamma_p - 1)/(M_p \nu)}{3(\gamma_p - 1)(\gamma_g - 1)} \right]^{1/2} \left(\frac{T}{\mathrm{keV}} \right) (\rho r)_{\mathrm{hs}}^{3/2} g_i^{3/2}, \tag{20}$$

where M_p is the mass of the pusher in μg at the peak implosion velocity [17], which is the sum of the total mass of the DT fuel and the mass of the remaining ablator, and γ_p is the adiabatic index of the pusher. The average areal density of the hot spot $(\rho r)_{\mathrm{hs}}$ is in g/cm^2. The parameter $\nu \equiv \eta A_{\mathrm{DT}} V_{\mathrm{imp}}^2 / (2RT)$, where η is an implosion efficiency coefficient [17]. The neutron yield of an asymmetric capsule is

$$Y_n^i \approx 2.8 \times 10^6 g_i \frac{(\gamma_p - 1)(\gamma_g - 1)}{(3\gamma_p - 1)} \left(\frac{M_p}{\mu\mathrm{g}} \right)$$

$$\times \left(\frac{V_{\mathrm{imp}}}{\mathrm{km/s}} \right)^2 \left(\frac{P_{\mathrm{hs}} \tau_B}{\mathrm{Gb \cdot ns}} \right) T_{\mathrm{keV}}^2, \tag{21}$$

where Gb stands for gigabar and τ_B is the temporal burn width.

From this analysis, it follows that implosion asymmetry and hot-spot shape directly affect the alpha-heating and ther-

modynamic properties of the hot spot and, in turn, affect the thermonuclear burn of the capsule. Both the hot-spot pressure and the neutron yield would decrease as the implosion departs from spherical symmetry. The degradation in capsule performance due to implosion asymmetry can be quantified by the geometric shape function g_i. For a given fuel adiabat, the neutron yield of the capsule scales as $Y \propto (\rho r)_{\mathrm{hs}} T^{2.5}$ [17,18]. Thus, the ratio of the neutron yield between asymmetric and spherical hot spots can be quantified by the geometric shape function g_i,

$$Y_n^i / Y_n^{\mathrm{1D}} = \tau_h^i / \tau_0 = g_i, \tag{22}$$

where Y_n^{1D} is the neutron yield for a 1D spherical hot spot.

The neutron-yield degradation from implosion asymmetry is divided into two parts,

$$\Delta Y_n^i = Y_n^i \left(\frac{\Delta Y_n^{\mathrm{1D}}}{Y_n^{\mathrm{1D}}} + \frac{\Delta g_i}{g_i} \right). \tag{23}$$

The first term accounts for the degradation of the 1D spherical hot spot because of the decreased hot-spot pressure, density, and temperature caused by the asymmetric implosion, which can be viewed as an indirect effect of the shape. The second term accounts for the direct impact of the geometric shape of the hot spot because of the shorter hydrodynamic disassembly time and the decreased alpha-particle energy depositions. Equation (23) shows that given P_2/P_0, the degradation or effects of hot-spot shape on capsule performance increase with the neutron yield of the capsules, although the relative yield degradation percentage remains the same. The explicit shape effects for most of the low-yield low-foot experiments conducted at NIF are small because the impact on thermonuclear burn from a low hot-spot areal density is larger than the impact from the hot-spot shape and the alpha-heating in these shots was very minimal. Consequently, implosion asymmetry is not a major cause of poor performance of these shots.

V. COMPARISONS WITH EXPERIMENTAL DATA

With the measurable shape function g_i, we are able to evaluate the effects of implosion asymmetry on the thermonuclear burn of a capsule by comparing our theoretical predictions with the experimental data from NIF. In Fig. 2, we plot the ratio of the capsule yield to the 1D capsule yield as a function of the aspect ratio c/a, showing that the neutron yield decreases as the hot-spot shape departs from a sphere. The 1D capsule yield is calculated by the yield formula, (21) [18,19], which uses the peak implosion velocity, hot-spot areal density derived from the minimal energy implosion scaling model [17], fuel adiabat, neutron down-scatter ratio (DSR), and hot-spot temperature. Figure 2 shows that hot spots with a prolate shape (sausage) perform better than hot spots with an oblate shape (pancake). This theoretical result is consistent with the NIF ignition experimental data [27,28] and numerical simulations [14,29].

Generally, hot spots with toroidal shapes have the most degraded performance. Our theory indicates that prolate hot spots suffer less yield degradation than either oblate or toroidal hot-spot shapes for any value of P_2/P_0. As $|P_2/P_0|$ reaches 0.4, an oblate hot spot turns into a toroidal shape and a prolate hot spot turns into a dipole shape.
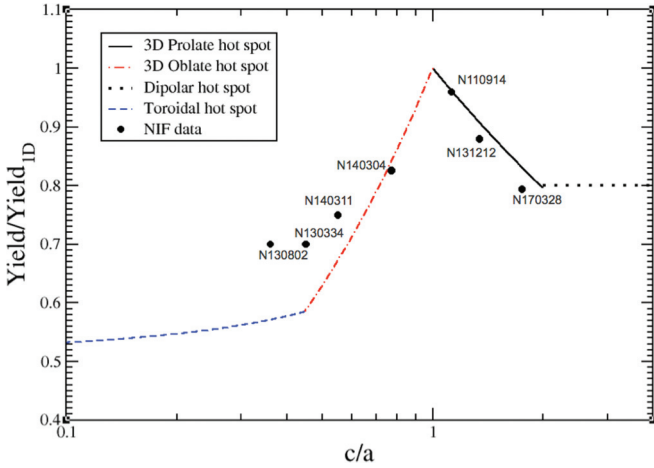
FIG. 2. Theoretical yield degradation due to the various hot-spot shapes. Equations (12) and (22) show that an implosion with a prolate hot-spot shape is less degraded than one with an oblate or a toroidal shape. Degradation in the various cases is plotted: 3D prolate (solid black line), 3D oblate (dot-dashed red line), toroidal (dashed blue line), and dipole (dotted black line). NIF experimental data are plotted in black dots.

Hot-spot shapes are measured in NIF experiments with modes up to M_4 and P_4. For this article, we analyzed 64 shots performed at NIF [30]. The measured neutron yields in these shots range from 8×10^{13} to 9×10^{15}, and P_2/P_0 ranges from -0.68 to 0.41. In the following analysis, we apply our theory to the NIF data to quantify the degradation in neutron yield due to implosion asymmetry or hot-spot shape. We then compare the degraded performance with the observed yield of the capsule.

Figure 3 demonstrates that shape effects are relatively more noticeable for neutron yields $>10^{14}$ by comparing the experimental yield with the 1D yields from Eqs. (21) and (22). This is because the values of yield degradation due to geometric
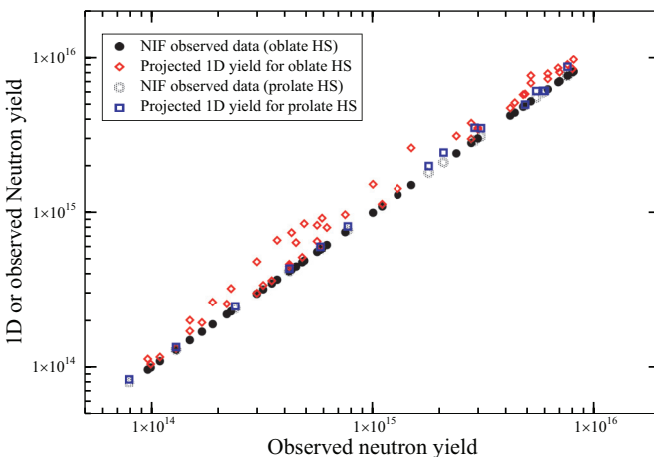

FIG. 3. Comparison between the neutron yields of the 1D (spherical hot spot) capsule from Eq. (A2) and the NIF experimental data shows that shape effects become important when the yield is above 10^{14} and alpha-heating becomes important. Red diamonds and blue squares represent the projected 1D capsule performance for oblate and prolate hot spots, respectively, if they were all spherical. Filled black circles represent NIF data with oblate hot spots; open black circles, NIF data with prolate hot spots.

TABLE I. Selected NIF shots and their measured physical quantities. The relationship between the total areal density of the DT fuel and the measured neutron down-scatter ratio (DSR) is approximately $(\rho r)_{\text{tot}} \simeq 21 \times \text{DSR}$ [10].

Shot No.	V_{imp} (km/s)	P_2/P_0	DSR (%)	T_i (keV)	Y_{ob} ($\times 10^{15}$)
N140225	333	0–0.02	3.88	4.52	2.80
N110914	355	0.08	4.9	3.49	0.58
N131212	331	0.21	2.5	2.81	2.30
N170328	380	0.41	3.6	4.2	5.00
N140311	372	-0.35	4.32	5.38	5.18
N140304	380	-0.17	3.4	5.85	8.10
N130802	329	-0.54	2.63	2.85	0.48

shape depend explicitly not only on the shape parameters but also on the capsule yield as shown in Eq. (23). So the values of yield degradation for high-yield capsules would be more visible than that for low-yield capsules if the hot-spot shapes were similar although the percentages of degradation were the same. In the figure, red diamonds represent the 1D neutron yield of the capsules when the hot spots were spherical instead of oblate and blue squares show the 1D neutron yield of the capsules when the hot spots were spherical instead of prolate. With the NIF data the degradation of the thermonuclear burn due to hot-spot shape indeed is shown to increase with the yield of the capsule with similar hot-spot shapes. The shape effect was even more obvious in some capsules with yields below 10^{15} as shown Fig. 3, because the decreased hydrodynamic disassembly time due to implosion asymmetry resulted in a significant reduction in alpha-heating and hence the neutron yield [19]. As the implosion symmetry improves, the hydrodynamic disassembly time is lengthened, and then the alpha-particle deposition and heating in the hot spot become appreciable, leading to a higher capsule performance as shown in the upper-right corner of Fig. 3, where the high-yield capsules seem less sensitive to shape. Across all NIF shots, the maximum yield degradation was about 20% for prolate hot spots and 45% for oblate hot spots.

For in-depth comparison and analysis, we take seven NIF shots as examples. These shots were selected because there is a complete set of nuclear data and x-ray and neutron images of the hot spots. Each shot represents one of the four typical hot-spot shapes. Six are high-foot shots, which had high design fuel adiabats [31,32]. Table I details shot information and measured physical quantities, including the peak implosion velocity V_{imp}, neutron down-scatter ratio (DSR), ion temperature (T) of the hot spot, and observed neutron yield (Y_{ob}) of the capsule.

Applying our shape theory to these shots, using the measured P_2/P_0 listed in Table I, the predicted capsule performance for each capsule in one, two, and three dimensions is listed in Table II. The comparison with the experimental data is clearly improved when the shape deviation is taken into account with Eqs. (22) and (23).

VI. CONCLUSIONS

In conclusion, we have developed an analytical model to quantify the effects of implosion symmetry on the ignition and

TABLE II. Comparison between predicted and observed neutron yields, in units of $\times 10^{15}$. In this table, we have used 5/3 for the adiabatic index of the DT fuel.

Shot No.	Hot-spot shape	Y_n^{1D}	Y_n^{2D}	Y_n^{3D}	Y_{ob}
N140225	Sphere	2.6	—	—	2.80
N110914	Sphere	0.61	—	—	0.58
N131212	Prolate	2.8	2.41	2.5	2.30
N170328	Prolate	6.3	5.3	5.8	5.00
N140311	Oblate	6.7	5	4.5	5.18
N140304	Oblate	9.8	8.55	8.2	8.10
N130802	Torus	0.7	—	0.36	0.48

burn of NIF capsules in terms of the measurable symmetry quantity P_2/P_0. Five possible hot-spot shapes with symmetry along the axis of the hohlraum have been considered: spherical, oblate, prolate, toroidal and dipolar hot spots. We found that toroidal hot-spot shapes cause the most degradation in performance relative to 1D spherical hot spots and that prolate hot spots have the least effect. An oblate hot spot will turn into a toroidal hot spot when $P_2/P_0 < -0.4$. Similarly, a prolate hot spot will turn into a dipole at $P_2/P_0 > 0.5$. We applied our analytical models [17–20] to analysis of the ICF experiments performed at NIF, including both low-foot and high-foot capsule experiments. Our model predictions are consistent with the experimental data.

Our study shows that (i) the shape effect on the capsule hydrodynamic disassembly time causes the degradation of the capsule performance due to implosion asymmetry; (ii) the variations of the hydrodynamic disassembly time with hot-spot shape differentiate the yield degradation with respect to different hot-spot shapes, for example, prolate, oblate, toroidal, and dipolar; (iii) the shape effect is negligible for shots with a yield $< 10^{14}$ because the hot spots in these shots are generally poorly compressed and the impact of the shape effect on thermonuclear burn is relatively small compared to the impact of a low hot-spot areal density; (iv) shape effects become more noticeable when the neutron yield is higher than 3×10^{14} because the decreased hydrodynamic disassembly time due to shape can significantly reduce the alpha-particle heating in the hot spot; and (v) deformed hot spots would require more internal energy to achieve ignition than 1D spherical hot spots.

For most of the NIF shots, the maximum negative impact on thermonuclear burn due to hot-spot shape to date is less than 20% for prolate and 45% for oblate. These results are very consistent with the numerical simulations performed by Kawata *et al.* [2] more than three decades ago.

APPENDIX

In a more general situation, such as when P_4 and M_4 are not negligible, we can express the dimensionless ratio r_{min}/r_0 of a 3D hot spot in spherical harmonics,

$$\frac{r_{min}}{r_0} = \tilde{h}^{1/3} g_{3D}, \tag{A1}$$

where $\tilde{h}$ is a function of P_2, P_4, and M_4 (M_m, $m = 1, 2, \ldots$ is the harmonic expansion in the polar view) and has the approximate expression [33]

$$\tilde{h} = c_1^2(c_1 + c_2) + \left(\frac{3c_1}{5} + \frac{c_3}{3}\right)(c_1 c_3 + c_2^2)$$
$$+ \frac{c_2(6c_1 c_3 + c_2^2)}{7} + c_3^2\left(\frac{3c_2}{11} + \frac{c_3}{13}\right)$$
$$+ \frac{64 c_4^2}{105}\left(c_1 + \frac{c_2}{11} + \frac{3c_3}{143}\right). \tag{A2}$$

The coefficients are given by $c_1 = 1 - (P_2/P_0)/2 + 3(P_4/P_0)/8$, $c_2 = 3[P_2/P_0 - 5(P_4/P_0)/2]/2$, $c_3 = 35(P_4/P_0)/8$, and $c_4 = [1 - (P_2/P_0)/2 + 3(P_4/P_0)/8](M_4/M_0)$. For convenience, in this article, we focus on the impacts of P_2 only. Neglecting terms higher than P_2 gives $\tilde{h} \simeq 1 + 12(P_2/P_0)^2/20 \simeq 1$.

[1] M. H. Emery, J. H. Orens, J. H. Gardner, and J. P. Boris, Phys. Rev. Lett. **48**, 253 (1982).

[2] S. Kawata and K. Niu, J. Phys. Soc. Jpn. **53**, 3416 (1984).

[3] S. Kawata, T. Karino, and A. I. Ogoyski, Matter Radiat. Extremes **1**, 89 (2016).

[4] D. S. Clark, M. M. Marinak, C. R. Weber, D. C. Eder, S. W. Haan, B. A. Hammel, D. E. Hinkel, O. S. Jones, J. L. Milovich, P. K. Patel, H. F. Robey, J. D. Salmonson, S. M. Sepke, and C. A. Thomas, Phys. Plasmas **22**, 022703 (2015).

[5] D. S. Clark, C. R. Weber, J. L. Milovich, J. D. Salmonson, A. L. Kritcher, S. W. Haan, B. A. Hammel, D. E. Hinkel, O. A. Hurricane, O. S. Jones, M. M. Marinak, P. K. Patel, H. F. Robey, S. M. Sepke, and M. J. Edwards, Phys. Plasmas **23**, 056302 (2016).

[6] C. R. Weber, D. S. Clark, A. W. Cook, D. C. Eder, S. W. Haan, B. A. Hammel, D. E. Hinkel, O. S. Jones, M. M. Marinak, J. L. Milovich, P. K. Patel, H. F. Robey, J. D. Salmonson, S. M. Sepke, and C. A. Thomas, Phys. Plasmas **22**, 032702 (2015).

[7] V. N. Goncharov, T. C. Sangster, R. Betti, T. R. Boehly, M. J. Bonino, T. J. B. Collins, R. S. Craxton, J. A. Delettrez, D. H. Edgell, R. Epstein, R. K. Follett, C. J. Forrest, D. H. Froula, V. Yu. Glebov, D. R. Harding, R. J. Henchen, S. X. Hu, I. V.

Igumenshchev, R. Janezic, J. H. Kelly, T. J. Kessler, T. Z. Kosc, S. J. Loucks, J. A. Marozas, F. J. Marshall, A. V. Maximov, R. L. McCrory, P. W. McKenty, D. D. Meyerhofer, D. T. Michel, J. F. Myatt, R. Nora, P. B. Radha, S. P. Regan, W. Seka, W. T. Shmayda, R. W. Short, A. Shvydky, S. Skupsky, C. Stoeckl, B. Yaakobi, J. A. Frenje, M. Gatu-Johnson, R. D. Petrasso, and D. T. Casey, Phys. Plasmas **21**, 056315 (2014).

[8] C. K. Li, F. H. Seguin, J. A. Frenje, M. J. Rosenberg, H. G. Rinderknecht, A. B. Zylstra, R. D. Petrasso, P. A. Amendt, O. L. Landen, A. J. Mackinnon, R. P. J. Town, S. C. Wilks, R. Betti, D. D. Meyerhofer, J. M. Soures, J. Hund, J. D. Kilkenny, and A. Nikroo, Phys. Rev. Lett. **108**, 025001 (2012).

[9] A. Bose, R. Betti, D. Shvarts, and K. W. Woo, Phys. Plasmas **24**, 102704 (2017).

[10] S. W. Haan, J. D. Lindl, D. A. Callahan, D. S. Clark, J. D. Salmonson, B. A. Hammel, L. J. Atherton, R. C. Cook, M. J. Edwards, S. Glenzer, A. V. Hamza, S. P. Hatchett, M. C. Herrmann, D. E. Hinkel, D. D. Ho, H. Huang, O. S. Jones, J. Kline, G. Kyrala, O. L. Landen, B. J. MacGowan, M. M. Marinak, D. D. Meyerhofer, J. L. Milovich, K. A. Moreno, E. I. Moses, D. H. Munro, A. Nikroo, R. E. Olson, K. Peterson, S. M. Pollaine, J. E. Ralph, H. F. Robey, B. K. Spears, P. T. Springer, L. J. Suter, C. A. Thomas, R. P. Town, R. Vesey, S. V. Weber, H. L. Wilkens, and D. C. Wilson, Phys. Plasmas **18**, 051001 (2011).

[11] F. E. Merrill, C. R. Danly, D. N. Fittinghoff, G. P. Grim, N. Guler, P. L. Volegov, and C. H. Wilde, J. Phys.: Conf. Ser. **688**, 012064 (2016).

[12] R. Kishony and D. Shvarts, Phys. Plasmas **8**, 4925 (2001).

[13] P. Springer (private communication, March, 2017).

[14] J. P. Chittenden, B. D. Appelbe, F. Manke, K. McGlinchey, and N. P. L. Niasse, Phys. Plasmas **23**, 052708 (2016).

[15] I. V. Igumenshchev, V. N. Goncharov, F. J. Marshall, J. P. Knauer, E. M. Campbell, C. J. Forrest, D. H. Froula, V. Yu. Glebov, R. L. McCrory, S. P. Regan, T. C. Sangster, S. Skupsky, and C. Stoeckl, Phys. Plasmas **23**, 052702 (2016).

[16] J. Hammer (private communication, March, 2017).

[17] B. Cheng, T. J. T. Kwan, Y.-M. Wang, and S. H. Batha, Phys. Rev. E **88**, 041101 (2013).

[18] B. Cheng, T. J. T. Kwan, Y.-M. Wang, and S. H. Batha, Phys. Plasmas **21**, 102707 (2014).

[19] B. Cheng, T. J. T. Kwan, Y. M. Wang, F. E. Merrill, C. J. Cerjan, and S. H. Batha, Phys. Plasmas **22**, 082704 (2015).

[20] B. Cheng, T. J. T. Kwan, Y. M. Wang, S. A. Yi, S. H. Batha, and F. J. Wysocki, Phys. Plasmas **23**, 120702 (2016).

[21] B. Cheng, T. J. T. Kwan, Y. M. Wang, S. A. Yi, S. H. Batha, and F. Wysocki, Plasma Phys. Control. Fusion **60**, 074011 (2018).

[22] O. N. Krokhin and V. B. Rozanov, Sov. J. Quantum Electron. **2**, 393 (1973).

[23] G. S. Fraley, E. J. Linnebur, R. J. Mason, and R. L. Morse, Phys. Fluids **17**, 474 (1974).

[24] R. Tipton, Private communications and preprint, Generalized Lawson Criteria for Inertial Confinement Fusion (Lawrence Livermore National Laboratory, Livermore, CA, 2015).

[25] G. R. Caughlan and W. A. Fowler, At. Data Nucl. Data Tables **40**, 283 (1988).

[26] H.-S. Bosch and G. M. Hale, Nucl. Fusion **32**, 611 (1992).

[27] T. Ma, presentation at ICF Physics Integration Meeting, 15 August 2014.

[28] P. Patel, presentation at Fuel Assembly Working Group, 8 October 2013.

[29] J. L. Peterson, K. D. Humbird, J. E. Field, S. T. Brandon, S. H. Langer, R. C. Nora, B. K. Spears, and P. T. Springer, Phys. Plasmas **24**, 032702 (2017).

[30] O. L. Landen, NIF data spreadsheet: Landen Top Level Summaries 12-05.xlsx (2017).

[31] D. S. Clark, D. E. Hinkel, D. C. Eder, O. S. Jones, S. W. Haan, B. A. Hammel, M. M. Marinak, J. L. Milovich, H. F. Robey, L. J. Suter, and R. P. J. Town, Phys. Plasmas **20**, 056318 (2013).

[32] C. J. Cerjan, P. T. Springer, and S. M. Sepke, Phys. Plasmas **20**, 056319 (2013).

[33] J. A. Koch, LLNL Report LLNL-TR-510411, Lawrence Livermore National Laboratory, Livermore, CA, 2011.